Langmuir

Article

pubs.acs.org/Langmuir

Understanding Stöber Silica's Pore Characteristics Measured by Gas Adsorption

Shanshan Li,[†,‡,§] Quan Wan,*[,†] Zonghua Qin,[†] Yuhong Fu,[†,‡] and Yuantao Gu[†,‡]

[†]State Key Laboratory of Ore Deposit Geochemistry, Institute of Geochemistry, Chinese Academy of Sciences, Guiyang, Guizhou 550002, China

[‡]University of Chinese Academy of Sciences, Beijing 100049, China

[§]School of Chemistry and Materials Science, Guizhou Normal University, Guiyang, Guizhou 550001, China

Supporting Information

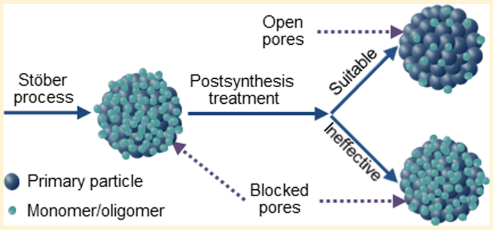

ABSTRACT: Controversial reports regarding Stöber silica's microporosity and specific surface area remain in the literature despite decades of widespread applications. In this work, Stöber silica samples prepared under controlled reaction time and postsynthesis washing/drying conditions were characterized by nitrogen adsorption at 77 K, transmission electron microscopy, elemental analysis, Fourier transform infrared spectroscopy, thermal analysis, and evolved gas analysis. Our experimental results demonstrated the important but often overlooked effects of reaction time and postsynthesis treatments on Stöber silica's pore characteristics, as evidenced by the strikingly large range of BET specific surface area (11.3–309.7 m^2/g). A simple micropore filling and blocking mechanism compatible with an existing Stöber silica growth model incorporating both aggregation and monomer addition steps was proposed to explain all our experimental findings. The carbon and nitrogen contents appear to serve well as the indicative link between our experimental variables and the resulting pore blocking by TEOS and its derivatives. A suitable combination of experimental conditions is recommended in order to make microporous Stöber silica samples with large specific surface area, including a short reaction time, water washing, and drying at moderate temperature preferably under vacuum.

1. INTRODUCTION

Nanoporous structures are ubiquitously found in the natural environment (e.g., in minerals, rocks, soils, sediments, organic matter, organisms, etc.) and significantly contribute to total surface area of porous geological media.[1,2] Fluids confined in nanoporous volume exhibit interesting size-dependent properties,[3−5] which affect many essential geochemical processes such as dissolution, sorption, diffusion, and reactivity of chemical substances within nanopores.[2] Accordingly, critical involvements of nanopores have been demonstrated in many fundamental earth and environment-related topics including chemical weathering,[6] ion adsorption/transport,[1] organic carbon preservation/availability,[7] shale gas evolution,[8] geological storage of carbon dioxide,[9] environmental pollution and control,[10] etc. Partly because of silica's dominant abundance in the earth's crust, laboratory studies concerning the roles of nanopores in earth science problems often selected synthetic nanoporous silica materials as model systems.[11−14] Our interest in pore size effect on the sorption behavior of nanopores (especially micropores, i.e., <2 nm) led us to a closer look at the Stöber silica material synthesized through an ammonia-catalyzed sol-gel process.[15] Owing to its regular spherical shape and well-controlled external particle size, Stöber silica has enjoyed versatile applications ranging from particulate functional materials to photonic crystals.[16] In order to utilize Stöber silica as a model sorbent, a clear understanding of its internal porous structure is of indispensable importance. Yet, despite Stöber silica's decades of notable applications, our literature survey surprisingly revealed inconsistent and sometimes contradictory descriptions of its pore characteristics.[17]

For instance, characterizations of Stöber silica samples generated a wide range of specific surface area (SSA) results, which appeared to be overly sensitive to the employed techniques. The conventional nitrogen adsorption measurement at 77 K often showed a BET specific surface area (S_{BET}) of Stöber silica slightly larger than the geometric surface area of the particles, which normally suggested a nonporous structure.[18−20] However, methods such as pycnometry, acid–base titration, liquid-phase adsorption, and small-angle X-ray scattering unanimously supported the existence of microporosity inside Stöber silica particles.[18,19,21−23] Using various experimental methods to characterize the same Stöber silica sample, Szekeres et al. found that the SSA results (10–24 m^2/g based on different models) from N_2 adsorption at 77 K were 20–30 times smaller than those (up to 670 m^2/g) derived from other methods performed at higher temperature.[18] Although it is unnecessary to seek a "perfect agreement" between results from different models,[24] difficulties in reconciling such divergent results clearly indicated a critical need for an

Received: October 24, 2014
Revised: December 2, 2014
Published: December 16, 2014

DOI: 10.1021/la5042103
Langmuir 2015, 31, 824−832

improved understanding of Stöber silica's complex microstructure.

On the other hand, even the same "standard" N_2 adsorption method at 77 K may produce highly contrasting SSA results for Stöber silica samples. Besides the aforementioned S_{BET} comparable to the geometric surface area, much larger S_{BET} results were also reported including 369 m^2/g for a Stöber silica with a particle diameter of ~42 nm,[25] 240 m^2/g (diameter ~730 nm),[21] and 324 m^2/g (diameter ~670 nm),[26] respectively. In a study where several Stöber silica samples were prepared and characterized under seemingly the same condition, the authors found it puzzling to explain the large variation in S_{BET} values spanning from a few to over 200 m^2/g.[21] While no thorough discussion was available to account for these scattered SSA results of the same type of material characterized with the same technique, many studies just routinely applied the BET method to obtain the surface area results. Occasionally, inadvertent use of SSA data might lead to severely misleading interpretations of Stöber silica's surface and pore-related properties. For example, compared with the commonly-accepted surface silanol group density (4−5 sites/nm^2) of amorphous silicas,[27] inconsistently large range and unrealistically high values (5.7−56 sites/nm^2) of surface functional group (silanol or charge) density could be derived if simply combining S_{BET} results and thermogravimetric or acid−base titration data.[28]

We are motivated to investigate the inconsistencies and contradictions on the surface area characterization of Stöber silica. Previously, many research studies focused on controlling size, size distribution, and shape of Stöber silica particles through varying synthetic conditions such as concentration of reactants, solvents, temperature, etc.[29−31] Nucleation and growth mechanisms of Stöber silica have also been extensively studied.[32−38] Much less work has been devoted to correlate the process conditions with the pore characteristics. In this work, we intended to bring attention to the previously overlooked effect of process conditions including the postsynthesis treatments on the Stöber silica's pore characteristics and thus to some extent clarify the long-standing problems involved in the pore characterizations. Specifically, we synthesized samples using the typical Stöber method and treated the samples through systematically controlled washing and drying conditions. We demonstrated the importance of the postsynthesis treatments in controlling the Stöber silica's pore structure as revealed by the SSA results measured by the N_2 adsorption (77 K) method and further suggested that this largely ignored effect could in fact be reconciled with an existing nucleation and growth mechanism for Stöber silica.

2. EXPERIMENTAL SECTION

2.1. Materials. Tetraethyl orthosilicate (TEOS, 96%) was purchased from TCI (Shanghai) Development Co., Ltd., China. Ethanol (99.7%) was purchased from Sinopharm Chemical Reagent Company, China. Ammonia (~26.5%) was from Chongqing Chuanjiang Chemical Reagent Company, China. All these chemicals were used without further purification. Deionized water was obtained from a Millipore synergy UV system (resistivity, 18.2 MΩ·cm).

2.2. Synthesis of Stöber Silica. A simple procedure briefly described below was followed to synthesize our Stöber silica samples. A mixture containing 18 mL of ammonia, 55 mL of deionized water, and 398 mL of ethanol was stirred in a flask under room temperature (~25 °C) for about 30 min. Subsequently, 29 mL of TEOS was quickly added to the mixture which was continuously stirred for an additional reaction period (1 or 3 h). The equivalent molar ratio for $TEOS:NH_3:H_2O$ was about 0.25:0.5:7.5 assuming all the mixed liquid volumes were additive. After reaction, the suspension was centrifuged at 10 000 rpm to collect the precipitate of silica particles.

2.3. Postsynthesis Treatments of Stöber Silica. The collected silica product was divided into several samples which were subject to washing with different solvents, i.e., deionized water only, ethanol only, or ethanol plus deionized water. Most samples were washed five times with either ethanol or water, while one sample was washed with ethanol twice and then deionized water three times. Each washing cycle was performed using a vortex mixer for 2 min, and after that the suspension was centrifuged and separated by decanting the supernatant liquid. Samples after washing were then dried at different temperatures (i.e., 50, 120, or 200 °C), for different durations (2 or 8 h), and with or without vacuum. The detailed process conditions for all the samples are summarized in Table 1.

Table 1. Sample Coding Based on Reaction Time and Postsynthesis Treatment

sample	reaction time (h)	washing solvent	drying temperature (°C)	drying time (h)
E1	1	ethanol	50	2
E2	1	ethanol	120	2
E3	1	ethanol	200	2
E4	1	ethanol	120va	8
W1	1	deionized water	50	2
W2	1	deionized water	120	2
W3	1	deionized water	200	2
W4	1	deionized water	120va	8
EW	1	ethanol + deionized water	120	2
E5	3	ethanol	120va	8
W5	3	deionized water	120va	8

[a] Drying under vacuum.

2.4. Characterizations of Post-treated Samples. The size and shape of Stöber silica particles were characterized using a Transmission Electron Microscope (TEM; JEOL, JEM-2000FX II, Japan) operated at 160 kV. Particle size was obtained by analyzing at least 200 particles using the ImageJ (US National Institutes of Health) software.

The carbon and nitrogen contents of all samples were determined by a combustion method (~1200 °C, in oxygen) using an elemental analysis instrument (vario MACRO cube, Elementar Analysensysteme GmbH, Germany). The result for each sample (20−50 mg) was the average value of two measurements.

The gas adsorption isotherms of N_2 (99.999% purity; 0.162 nm^2 molecular cross-sectional area; p/p_0 range 10^{-7} ~ 0.99) at 77 K were measured using a gas adsorption analyzer (Autosorb-iQ_2-MP, Quantachrome, Boynton Beach, FL). Before measurement, the powder sample was outgassed at 120 or 200 °C for up to 12 h under vacuum. BET (Brunauer−Emmett−Teller) and NLDFT (nonlocal density functional theory) models were used to obtain the specific surface area, pore size, pore volume, etc.

Thermogravimetry (TG) and differential scanning calorimetry (DSC) curves were determined using a simultaneous thermal analyzer (STA 449F3, NETZSCH, Germany). Each sample (20−30 mg) was heated from 50 to 1200 °C (10 °C/min heating rate) in a dry air atmosphere. Evolved gas analysis was performed by coupling STA with Fourier transform infrared spectroscopy (Vertex 70, Bruker, Germany). The infrared spectra of evolved gases were collected in the mid-infrared range (4000−400 cm^{-1}) using a resolution of 4 cm^{-1} and an accumulation of 16 scans.

3. RESULTS AND DISCUSSION

3.1. Characterization of Stöber Silica Particles. TEM micrographs of representative Stöber silica samples are shown in Figure 1a−f. While particles of all samples exhibit the typical

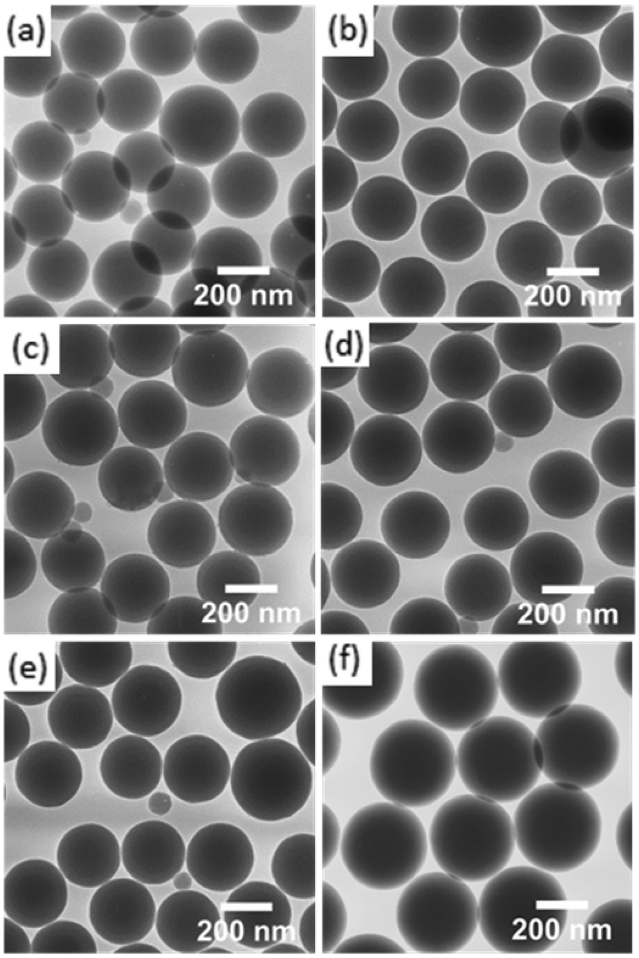

Figure 1. TEM pictures of samples: (a) E2, (b) E4, (c) W2, (d) W4, (e) EW, and (f) E5; scale bars: 200 nm, see Table 1 for sample coding (same below).

spherical shape, apparent differences can be found between samples with 1 or 3 h of reaction time. ImageJ analysis showed that an average particle diameter of ∼255 nm for samples with 1 h reaction time (Figure 1a−e), smaller than the diameter (∼330 nm) of those with 3 h reaction time (Figure 1f). Furthermore, some smaller particles were detected in samples with 1 h reaction time but not in samples with 3 h reaction time. These observations are consistent with a previously known self-sharpening growth pattern of Stöber process, in which particles with smaller diameters should grow faster than those with larger diameters.[33] Therefore, after sufficiently longer reaction time (3 h in our case), smaller particles could disappear by growing faster and a better monodispersity in size was achieved for samples E5 and W5. Another important observation is that when reaction time was the same, no discernible change in particle size or surface roughness was found due to postsynthesis treatments (washing or drying) under our experimental conditions (see Figure 1 and Table 1). Apparently, our postsynthesis treatments (unlike other harsh methods, e.g., alkaline etching) seemed mild enough to preserve the external size of the Stöber silica particles.

Nitrogen adsorption (77 K) isotherms were determined for all samples listed in Table 1. While the adsorption isotherms for samples W4 (see Figure 2b) and EW are classified as type I (according to IUPAC classification) indicating a microporous structure, most other samples (e.g., Figure 2a for sample E1) display a type II isotherm typical of a nonporous material.[39] Consistent with the type I isotherm, the pore size distribution of sample W4 derived from the NLDFT model (Figure 2c) shows a mean pore width of ∼1.2 nm within the micropore range. A common feature for all isotherms (as exemplified by Figure 2a,b) is the dramatic increase in the volume of adsorption at higher relative pressure (p/p_0 >0.97). This is attributed to the filling of interparticle pores by nitrogen molecules, which applies to all our samples with nanoscale external diameters. The results of gas adsorption analysis (based on BET and NLDFT models) including specific surface area, pore size, pore volume, etc., of all samples (some under different outgassing condition) are summarized in Table 2. Samples W4 and EW are shown to possess a microporous volume up to 0.1 cc/g, whereas the micropore volume for all other samples is negligible. For microporous samples (W4 and EW), the SSA from NLDFT is 11−13% larger than that from BET. In contrast, the S_{BET} is a few to over 30% larger than the SSA from NLDFT for all the other samples. The differences in SSA probably support that the more advanced NLDFT model can provide an estimation of SSA better than that of the classic BET model especially when both micropores and mesopores exist.[40] More importantly, no matter which method was used (BET or NLDFT), our results convincingly demonstrate the prominent effect of postsynthesis treatment condition on the SSA (ranging from ∼10 to >300 m^2/g), as well as a consistent overall trend regarding how the post-treatment conditions influence SSA values. Therefore, in our following discussion, we will mainly use the “standard” S_{BET} data to focus on the correlation between post-treatment and SSA results.

It is also worthy to point out that an obvious difficulty encountered in our experiment and many other previous studies[21,30] was the long equilibrium time to collect adsorption isotherms for microporous Stöber silica samples. For example, it took no more than 9 h to complete gas adsorption measurement for sample E1. However, for sample W4, about 30 days was taken to collect the data points, with a few points each taking 5 days to reach the equilibrium. The long measurement time might be associated with the quadrupole moment of the nitrogen molecule which tends to produce specific interaction at the gas−solid interface. Argon (Ar) adsorption at 87 K seems to be more suitable for many microporous systems, since the monatomic Ar molecule does not have any dipole or quadrupole moments and the higher bath temperature (87K) should facilitate gas diffusion in micropores.[41] Yet, it still took about 25 days to complete the Ar adsorption measurement (87 K) for sample W4, and the result is similar to that from the N_2 adsorption. It is perhaps reasonable to envisage a complex microporous structure (probably with narrow, tortuous inner pores, and clogging surface or inner barriers) in Stöber silica particles, which prevents nitrogen or argon molecules from quick entering and diffusing into the microporous system. This accessibility-based mechanism can also explain the observation (Figure 2b) that the desorption and adsorption branches did not meet at low relative pressures,[42] because it was hard to reach the adsorption/desorption equilibrium within short time in the narrow and clogging micropores. We further speculate that the required excessive adsorption time might have presented a substantial hurdle in some previous studies, leading to inconclusive or contradictory description of Stöber silica’s microporosity.

DOI: 10.1021/la5042103
Langmuir 2015, 31, 824−832

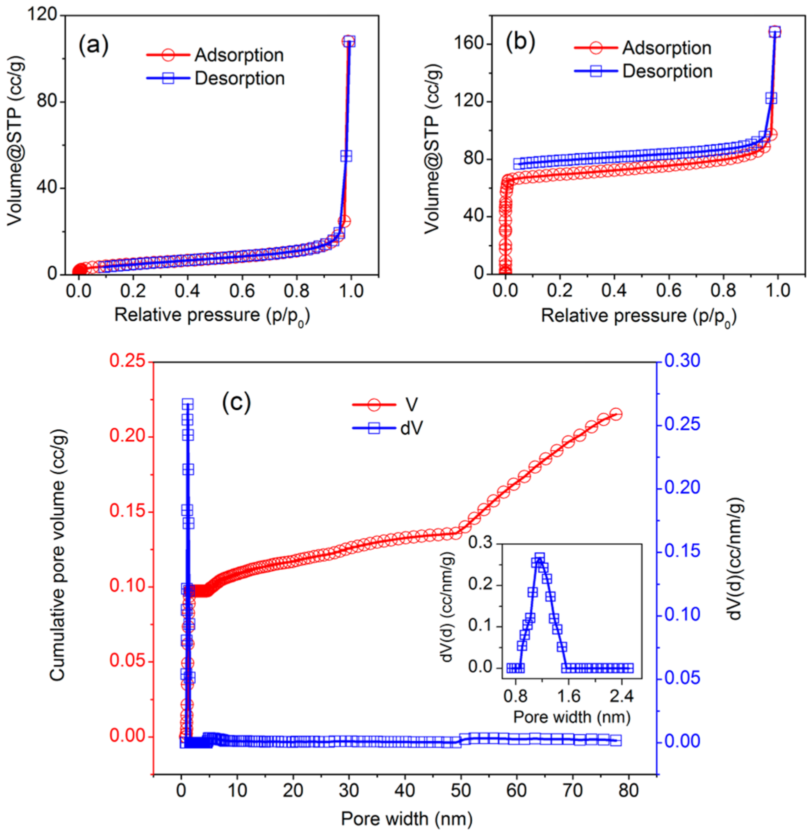

Figure 2. Gas adsorption (N_2 at 77 K) isotherms for (a) sample E1 and (b) sample W4. (c) Pore size distribution of sample W4 from NLDFT; the inset shows the pore size distribution below 2.5 nm.

Table 2. Specific Surface Area, Pore Size, and Pore Volume of Samples

			NLDFT				
sample	outgassing condition	S_{BET} (m^2/g)[a]	model type[b]	surface area (m^2/g)	pore width (nm)	pore volume (cc/g)	micropore volume (cc/g)[c]
E1	Δ[d]	13.2	III	10.3	3.7	0.017	0.000
E2	Δ	18.8	III	15.2	3.5	0.022	0.000
E3	Δ	18.0	III	15.1	3.5	0.022	0.000
E4	Δ	19.7	III	15.1	3.5	0.024	0.000
	▲[e]	18.0	III	14.3	3.5	0.022	0.000
W1	Δ	32.0	III	24.1	3.8	0.036	0.000
	▲	23.3	III	17.9	3.8	0.028	0.000
W2	Δ	33.7	III	32.3	1.2	0.033	0.004
	▲	32.0	III	24.2	3.5	0.036	0.000
W3	Δ	19.8	III	15.6	3.2	0.023	0.000
W4	Δ	309.7	I	346.8	1.2	0.215	0.097
EW	Δ	153.0	I	170.8	1.2	0.177	0.047
	▲	279.1	II	315.1	1.2	0.131	0.102
E5	Δ	11.3	I	8.7	5.9	0.022	0.000
W5	Δ	13.9	I	10.9	4.4	0.025	0.000

[a] Specific surface area calculated from BET model. [b] NLDFT offers three types of model for silica. Type I: cylinder pore, NLDFT adsorption branch model; type II: cylinder pore, NLDFT equilibrium model; type III: cylinder/sphere pore, NLDFT adsorption model. We chose the model with the least fitting error for each sample. [c] Micropore volume is the volume for pore size less than 2 nm. [d] Δ denotes outgassing at 100 °C for 0.5 h and then 200 °C for 12 h. [e] ▲denotes outgassing at 100 °C for 0.5 h and then 120 °C for 12 h.

3.2. Origin of Micropores and Effect of Reaction Time. Many mechanistic studies have been carried out, mainly aiming at explaining or controlling size and size distribution of Stöber silica particles. It is noteworthy that the micropore formation mechanism has an important role in the evolution of the Stöber silica growth model. First, the classic LaMer model was adopted since it could easily explain the uniform external size of Stöber particles.[38,43,44] In this model, a quick burst of the nucleation process takes place when the monomer concentration (from hydrolysis of TEOS) reaches a critical supersaturation level, and then particle growth proceeds via monomer addition to the nuclei. The particle size uniformity can be achieved as a consequence of the constant number of growing particles plus an intuitive self-sharpening growth mechanism, which stipulates

Table 3. Carbon and Nitrogen Contents of All Samples

sample	E1	E2	E3	E4	W1	W2	W3	W4	EW	E5	W5
carbon (wt %)	2.127	1.683	1.727	2.236	0.032	0.078	0.072	0.430	0.167	2.062	2.028
nitrogen (wt %)	1.491	0.158	0.011	0.042	1.030	0.259	0.007	0.060	0.140	0.120	0.114

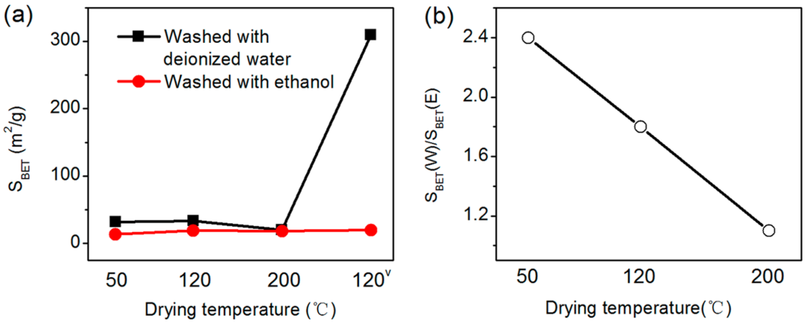

Figure 3. (a) S_{BET} of samples (1 h reaction time; 200 °C outgassing) with different washing solvent and drying temperature. (b) S_{BET} ratio between samples washed with water (W) and ethanol (E). The largest data point (15.7) for 120^v drying is omitted to enhance visual contrast.

a faster growth rate for smaller particles. Yet the LaMer model failed to explain the origin of micropores since particle growth through molecular addition cannot form porous structures. Bogush et al. proposed a different model, where aggregation of colloidal particles was considered the major growth pathway and colloidal stability played a key role in determining the final particle size and uniformity.[33,35] This aggregation model readily explains the granular appearance of Stöber particles as well as the 11−15% porosity based on bulk density measurement[29] and is further corroborated by SAXS, TEM, and NMR evidence indicating the existence of primary particles of a few nanometers in size.[32,37,45] A third model was also proposed which incorporates both aggregation and monomer-addition processes.[30,34,36] The aggregation process is still the major contribution to the particle growth, which also forms nanopores inside the Stöber silica particles. However, addition of monomers or small oligomers to the particle surface or shell may become the dominant process, after nucleation ceases to proceed because of lowered monomer concentration at the later stage of the reaction.

Apparently, the third model provides a more comprehensive description of the Stöber process, which also proves useful in explaining our experimental results. Although it may be hard to pinpoint the time when molecular addition becomes the dominant mechanism, the important point in the third model is that monomer addition happens at the later stage of particle growth. Since Stöber silica's micropores are formed by aggregation of small primary particles, the porous structure may be very complex (as mentioned before) with narrow size and tortuous shape. At the molecular growth stage, monomers or oligomers may be adsorbed or trapped onto the particle surface and block the entrance or possibly inner part of the micropores. Accordingly, it is reasonable to predict that the extent of pore blocking should increase with the reaction time. On the contrary, the pore clogging effect can be greatly relieved if the reaction is forced to stop before the dominant molecular addition stage.

To test the effect of the reaction time, we prepared samples under exactly the same synthetic condition except for different reaction duration (1 or 3 h). Using the external diameter and a bulk density of 1.9 g/cm^3,[3,21,22] the geometric surface areas for particles with 1 and 3 h of reaction time are calculated to be 12.4 and 9.6 m^2/g, respectively. Given suitable postsynthesis treatment, samples (W4 and EW in Table 2) with 1 h of reaction time present large SSA and a microporous structure. Nevertheless, the SSA of either sample E5 or W5 with 3 h of reaction time is just comparable to the geometric surface area of particles. Another interesting comparison can be seen from elemental analysis (C and N contents) results presented in Table 3. While water washing could efficiently reduce the carbon content (from incomplete hydrolysis of TEOS) of samples with 1 h reaction time, the carbon content of W5 remained at a high level (~2 wt %) after washing with water. These comparisons suggest that longer reaction time (3 h) promotes a firm nanopore blocking (by TEOS and its derivatives) which cannot be effectively cleared off by any postsynthesis treatment in our experiments. Our observations are also consistent with the results by Filipovic et al.,[26] who suggested that aging in the reaction mixture could enable efficient closing of pores. Since longer reaction time was commonly used to guarantee a better monodispersity in particle size, the above discussion may help understand why N_2 adsorption (77 K) measurement often indicated a nonporous structure of Stöber silica in many previous investigations.

3.3. Effect of Solvent Washing on Pore Structure. After Stöber silica product was separated from the synthetic mixture, it was normally washed using solvents such as ethanol or water. Since TEOS is immiscible in water but dissolves easily in ethanol,[46] ethanol was the preferred washing solvent in order to remove unreacted TEOS in a majority of investigations. Besides this obvious purpose, washing procedure in Stöber silica preparation was not adequately discussed. Our experimental results (see Table 2) surprisingly indicated that postsynthesis solvent washing played an effective role on the pore characterization results. Figure 3a presents a comparison of the S_{BET} results of samples with 1 h reaction time but washed with either ethanol or water and dried at different temperatures. It can be immediately seen (Figure 3a,b) that samples washed with water all show significantly higher S_{BET} values than the corresponding samples washed with ethanol. Specifically, the S_{BET} ratios (shown in Figure 3b) between samples washed with water (W) and ethanol (E) are calculated (data from Table 2) to be 2.4 (50 °C drying), 1.8 (120 °C drying), 1.1 (200 °C drying), and 15.7 (120 °C drying under vacuum), respectively. The fact that S_{BET} ratios vary with drying temperature also implies a profound effect of drying condition, which will be discussed in **3.4**. Furthermore, only samples W4 (highest point in Figure 3a) and EW with 1 h reaction time, water washing, and suitable drying conditions are able to produce large S_{BET} values indicating microporous structures.

Figure 4 shows the relationship between carbon content and post-treatment condition (drying and washing) of all samples except EW, E5, and W5. It is commonly recognized that C content of Stöber silica is in the form of the ethoxyl group (OC_2H_5) which stems from incomplete hydrolysis of TEOS.[47] The contribution of C% from residual ethanol molecules should be negligible even for samples synthesized and washed in ethanol medium (E1–4), since ethanol can be easily removed by drying (or outgassing). However, we do not exclude the possibility that several ethoxyl-containing species coexist in the sample, including OC_2H_5 chemically bonded to the silica skeleton and partly hydrolyzed TEOS (and its oligomers) physically trapped or adsorbed at the surface or in the pores. As shown in Figure 4, water (instead of ethanol) washing can efficiently remove carbon content of samples except W5 with longer reaction time (discussed earlier), while drying conditions appear to be a less effective factor. The FTIR transmission spectrum (see Figure S1 of the Supporting Information) also proves removal of carbon through water washing. It is clear that the C–H stretching vibration peak (2982 cm^{-1}) presented in sample E1 disappears in the spectrum of sample W4. Two pathways may describe how water removes carbon content through attacking the ethoxyl-containing species. Besides converting ethoxyl into volatile ethanol, it also hydrolyzes oligomers into a more acidic form with less mass, which becomes more soluble in water.

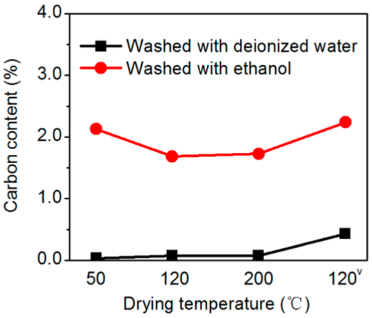

Figure 4. Carbon content of samples (1 h reaction time) with different washing and drying conditions.

Two pore-blocking mechanisms are possible to link the effect of solvent washing with pore characterization results. Since the size of ethoxyl group (OC_2H_5) is much larger than the silanol group (OH), the ethoxyl group itself may fill or block the narrow micropores (~1.2 nm according to NLDFT) or the pore throat where small primary particles aggregate. Unreacted TEOS monomers and oligomers may also be trapped at the pore entrance or pore channel. Both mechanisms can significantly hinder the entry or diffusion of N_2 molecules during gas adsorption (77 K) measurement, thus making the samples equivalently nonporous. Therefore, it appears reasonable to correlate the level of carbon content with the extent of pore clogging. When performing water washing, the above pore blocking mechanisms fail to work because of the two hydrolysis pathways discussed earlier. On the other hand, ethanol has no hydrolytic ability, and thus the S_{BET} results of ethanol-washed samples are considerably smaller than those of water-washed samples.

3.4. Effect of Drying and Outgassing Conditions. It is known that thermal history may affect pore structure of materials. Before gas adsorption measurement, our samples experienced two heating steps including drying and outgassing, both at reasonably "safe" temperature (≤200 °C). Surprisingly, our experiments with Stöber silica samples indicated a pronounced and complicated effect of drying condition (see Figure 3). As shown in Table 2 and Figure 3, the ethanol-washed samples (E series) follow an order E1 < E3 < E2 < E4 in terms of S_{BET}, with very close SSA values for E3, E2, and E4 (especially when S_{DFT} is used). The S_{BET} order for water-washed samples (W series) following W3 < W1 < W2 < W4 is much more distinguishable, with S_{BET}(W4) being 15 times larger than S_{BET}(W3).

To explain the above patterns, we first carried out thermal analysis coupled with evolved gas analysis of our samples (see Figure S2, Supporting Information). The extracted FTIR spectra (398 °C in Figure S2e and 454 °C in Figure S2f) confirm part of the weight loss in the form of CO_2 (absorption at 2250–2400 cm^{-1}), which was transformed under air atmosphere, from carbon content in each sample. The weight loss (between 200–1200 °C) for sample E1 (6.99%) is higher than that of sample W4 (5.19%) (see Figure S2a,b), consistent with the higher carbon content of sample E1. The difference in DSC peak shape from 200 to 600 °C (Figure S2a,b) may be indicative of different locations of carbon-containing species in the pore structure. The extracted FTIR spectrum at 145 °C in Figure S2e confirms the presence of ammonia (NH_3) in sample E1 with characteristic absorption peaks at 931 and 966 cm^{-1}. No obvious NH_3 absorption is found for sample W4 (Figure S2f), consistent with its reduced nitrogen content (Table 3) due to harsher drying conditions.

The difference in carbon content of our samples is mainly controlled by the choice of washing solvent instead of drying, as shown in Figure 4. However, Figure 5 shows that drying is the major factor controlling nitrogen content for both E and W series. Furthermore, as ammonia evolves at ~145 °C (Figure S2e), both series follow the same order of 3 < 4 < 2 < 1 in terms of nitrogen content as a consequence of different temperatures and vacuum conditions. Since N takes the form of NH_3, the catalytic function of ammonia should be helpful to decipher the link between S_{BET} and drying condition. It is known that condensation reactions of silanol or ethoxyl groups can be catalyzed by ammonia during Stöber synthesis at ambient temperature.[31] We argue that such catalytic reactions

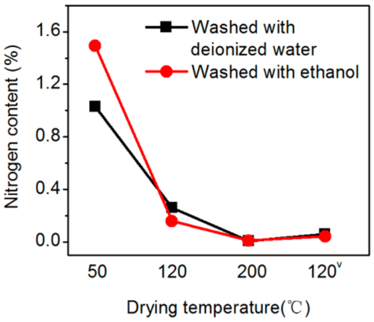

Figure 5. Nitrogen content of samples (1 h reaction time) with different washing and drying conditions.

still occur in powder form and can be promoted at higher temperature. Therefore, although dehydroxylation (condensation of silanols) at 200 °C may just take place according to the Zhuravlev model,[27] the extent of condensation is expected to be significantly higher in the presence of ammonia and especially at locations (e.g., narrow pore throats) with abundant vicinal silanol groups. Besides condensation of nearby silanols on the pore channel, the originally physically trapped monomers or oligomers may also condense with the silanols on the pore wall. The net effect of the above condensations is narrowed (or even closed) pores and more serious pore clogging, leading to smaller SSA results from gas adsorption characterization. The drying effect should be more pronounced in the W series since hydrolysis reactions supply more silanol groups for condensation, which is consistent with the comparison of the drying effect between the two series. It is also important to note that before drying, every sample should have a starting N content larger or at least comparable to that of E1 and W1 (1−1.5 wt %) dried at the lowest temperature (50 °C). For example, though sample W3 contains the least N content after drying at 200 °C, silanol condensation still happens during the drying process with the aid of ammonia (>1% N, initially) catalysis. Since 200 °C heating appears most efficient to promote ammonia-catalyzed silanol condensation, W3 shows the least S_{BET} (19.8 m^2/g) among the W series. Sample E1 (instead of E3) having the least S_{BET} among the E series may be related to its considerably higher carbon content.

Whereas higher temperature drying promotes NH_3-catalyzed condensation, drying also evaporates volatile NH_3, making the catalysis less effective. The balance between the above two counteracting effects probably explains the similar S_{BET} of samples W1 and W2 dried at moderate temperature (50 and 120 °C, respectively). Compared with sample W3 dried at 200 °C, although both samples W1 and W2 went through high outgassing temperature (200 °C), the ammonia content of W1 and W2 should be lower at the beginning of 200 °C heating and would be further lowered because of vacuum outgassing. Therefore, the extent of silanol condensation is still higher for W3 (thus with lower S_{BET}). Similarly, after being dried at 120 °C under vacuum for longer time (8 h), W4 contains less ammonia than W2 and thus shows the largest S_{BET} (309.7 m^2/g) due to the least extent of ammonia-catalyzed condensation.

We also prepared sample EW by incorporating washing with both ethanol and water and then drying at 120 °C. The S_{BET} (200 °C outgassing) of EW is 153.0 m^2/g, much larger than that (33.7 m^2/g) of W2 also dried at 120 °C. A synergistic effect which takes advantage of the different dissolving abilities from both solvents is possible. Yet, the fact that both the nitrogen content and S_{BET} value of sample EW lie in between those of samples W2 and W4 is highly indicative of the role of the ammonia catalysis mechanism (see Tables 2 and 3). When sample EW was outgassed at a lower temperature (120 °C), a large increase in S_{BET} value (from 153.0 to 279.1 m^2/g) was observed, which is again consistent with the drying temperature effect involving silanol condensation catalyzed with a certain amount of ammonia (only 0.14% in the case of EW). It appears hard to explain the different trend in S_{BET} of W1 and W2 when changing the outgassing temperature from 200 to 120 °C. Possibly, it is because that the gas adsorption measurement for the 120 °C outgassed W1 and W2 was performed two and half months after those outgassed at 200 °C because of the long measurement time (e.g., a month for W4) mentioned in section 3.1. It has been reported previously that long aging time (days or weeks) at room temperature could result in interparticle bonding and pore closing.[26,33]

4. CONCLUSIONS

We have demonstrated that the pore characteristics of Stöber silica can be significantly influenced by multiple factors including reaction time, washing solvent, drying condition, and outgassing temperature. A micropore filling and clogging mechanism is proposed to successfully explain the marked effects of reaction time and postsynthesis treatments observed in our study. In order to make microporous Stöber silica samples with large specific surface area, a proper combination of experimental variables is suggested including short reaction time, water washing, and drying at moderate temperature. Nitrogen adsorption (77 K) measurement coupled with BET or NLDFT model serves as a standard method to reasonably reveal the pore characteristics of Stöber silica material. Yet, the equilibrium time for microporous samples can be very long due to slow gas diffusion in the narrow and clogged pore channels, which is inefficient and may even cast doubt on the absolute results. Other pore characterization techniques at higher temperature including CO_2 adsorption (273 K), SAXS, and several wet methods may be considered depending on the intended applications. Our work helps explain the existing discrepancies in the literature regarding the specific surface area of Stöber silica and may further provide practical guidance in optimizing processes for preparing microporous materials.

■ ASSOCIATED CONTENT

Ⓢ Supporting Information

Additional infrared transmission spectra, STA curves, 3D FTIR spectra of evolved gas, and extracted FTIR spectra of evolved gas of samples E1 and W4. This material is available free of charge via the Internet at http://pubs.acs.org.

■ AUTHOR INFORMATION

Corresponding Author

*E-mail: wanquan@vip.gyig.ac.cn.

Notes

The authors declare no competing financial interest.

■ ACKNOWLEDGMENTS

Q.W. gratefully acknowledges support of this work by the Chinese Academy of Sciences (“Hundred Talents Program”), the National Natural Science Foundation of China (41473064), and the State Key Laboratory of Ore Deposit Geochemistry (SKLODG-ZY125-09).

■ REFERENCES

(1) Wang, Y. F.; Bryan, C.; Xu, H. F.; Gao, H. Z. Nanogeochemistry: Geochemical Reactions and Mass Transfers in Nanopores. *Geology* **2003**, *31* (5), 387−390.

(2) Wang, Y. F. Nanogeochemistry: Nanostructures, Emergent Properties and Their Control on Geochemical Reactions and Mass Transfers. *Chem. Geol.* **2014**, *378*, 1−23.

(3) Denoyel, R.; Pellenq, R. J. M. Simple Phenomenological Models for Phase Transitions in a Confined Geometry. 1: Melting and Solidification in a Cylindrical Pore. *Langmuir* **2002**, *18* (7), 2710−2716.

(4) Li, T. D.; Gao, J. P.; Szoszkiewicz, R.; Landman, U.; Riedo, E. Structured and Viscous Water in Subnanometer Gaps. *Phys. Rev. B* **2007**, *75* (11).

(5) Senapati, S.; Chandra, A. Dielectric Constant of Water Confined in a Nanocavity. *J. Phys. Chem. B* **2001**, *105* (22), 5106−5109.

(6) Hochella, M. F.; Banfield, J. F. Chemical Weathering of Silicates in Nature: A Microscopic Perspective with Theoretical Considerations. *Rev. Mineral.* **1995**, *31*, 353−406.

(7) Zimmerman, A. R.; Chorover, J.; Goyne, K. W.; Brantley, S. L. Protection of Mesopore-Adsorbed Organic Matter from Enzymatic Degradation. *Environ. Sci. Technol.* **2004**, *38* (17), 4542−4548.

(8) Loucks, R. G.; Reed, R. M.; Ruppel, S. C.; Jarvie, D. M. Morphology, Genesis, and Distribution of Nanometer-Scale Pores in Siliceous Mudstones of the Mississippian Barnett Shale. *J. Sediment. Res.* **2009**, *79* (11-12), 848−861.

(9) Rother, G.; Krukowski, E. G.; Wallacher, D.; Grimm, N.; Bodnar, R. J.; Cole, D. R. Pore Size Effects on the Sorption of Supercritical CO_2 in Mesoporous CPG-10 Silica. *J. Phys. Chem. C* **2012**, *116* (1), 917−922.

(10) Miller, A. W.; Wang, Y. Radionuclide Interaction with Clays in Dilute and Heavily Compacted Systems: A Critical Review. *Environ. Sci. Technol.* **2012**, *46* (4), 1981−1994.

(11) Wu, D.; Navrotsky, A. Small Molecule-Silica Interactions in Porous Silica Structures. *Geochim. Cosmochim. Acta* **2013**, *109*, 38−50.

(12) Wu, D.; Hwang, S.-J.; Zones, S. I.; Navrotsky, A. Guest-Host Interactions of a Rigid Organic Molecule in Porous Silica Frameworks. *Proc. Natl. Acad. Sci. U.S.A.* **2014**, *111* (5), 1720−1725.

(13) Farrell, J.; Reinhard, M. Desorption of Halogenated Organics from Model Solids, Sediments, and Soil under Unsaturated Conditions. 1. Isotherms. *Environ. Sci. Technol.* **1994**, *28* (1), 53−62.

(14) Xing, B. S.; Pignatello, J. J.; Gigliotti, B. Competitive Sorption between Atrazine and other Organic Compounds in Soils and Model Sorbents. *Environ. Sci. Technol.* **1996**, *30* (8), 2432−2440.

(15) Stöber, W.; Fink, A.; Bohn, E. Controlled Growth of Monodisperse Silica Spheres in the Micron Size Range. *J. Colloid Interface Sci.* **1968**, *26* (1), 62−69.

(16) Xia, Y. N.; Gates, B.; Yin, Y. D.; Lu, Y. Monodispersed Colloidal Spheres: Old Materials with New Applications. *Adv. Mater.* **2000**, *12* (10), 693−713.

(17) Jelinek, L.; Dong, P.; Rojaspazos, C.; Taibi, H.; Kovats, E. S. Study of the Stöber Reaction.1. Properties of Colloidal Silica Spheres Prepared via Alkoxide Hydrolysis. *Langmuir* **1992**, *8* (9), 2152−2164.

(18) Szekeres, M.; Toth, J.; Dekany, I. Specific Surface Area of Stöber Silica Determined by Various Experimental Methods. *Langmuir* **2002**, *18* (7), 2678−2685.

(19) Dekany, I.; Nemeth, J.; Szekeres, M.; Schoonheydt, R. Surfacial, Liquid Sorption and Monolayer-Forming Properties of Hydrophilic and Hydrophobic Stöber Silica Particles. *Colloid Polym. Sci.* **2003**, *282* (1), 1−6.

(20) Howard, A.; Khdary, N. Spray Synthesis of Monodisperse Sub-Micron Spherical Silica Particles. *Mater. Lett.* **2007**, *61* (8-9), 1951−1954.

(21) Labrosse, A.; Burneau, A. Characterization of Porosity of Ammonia Catalysed Alkoxysilane Silica. *J. Non-Cryst. Solids* **1997**, *221* (2-3), 107−124.

(22) Wan, Q.; Ramsey, C.; Baran, G. Thermal Pretreatment of Silica Composite Filler Materials. *J. Therm. Anal. Calorim.* **2010**, *99* (1), 237−243.

(23) Wells, J. D.; Koopal, L. K.; Keizer, A. d. Monodisperse, Nonporous, Spherical Silica Particles. *Colloids Surf., A* **2000**, *166*, 171−176.

(24) Rouquerolt, J.; Avnir, D.; Fairbridge, C. W.; Everett, D. H.; Haynes, J. H.; Pernicone, N.; Ramsay, J. D. F.; Sing, K. S. W.; Unger, k. K. Recommendations for the Characterization of Porous Solids. *Pure Appl. Chem.* **1994**, *66* (8), 1739−1758.

(25) Davis, P. J.; Deshpande, R.; Smith, D. M.; Brinker, C. J.; Assink, R. A. Pore Structure Evolution in Silica Gel during Aging/Drying. IV. Varying Pore Fluid pH. *J. Non-Cryst. Solids* **1994**, *167* (3), 295−306.

(26) Filipovic, R.; Obrenovic, Z.; Stijepovic, I.; Nikolic, L. M.; Srdic, V. V. Synthesis of Mesoporous Silica Particles with Controlled Pore Structure. *Ceram. Int.* **2009**, *35* (8), 3347−3353.

(27) Zhuravlev, L. T. The Surface Chemistry of Amorphous Silica. Zhuravlev Model. *Colloids Surf., A* **2000**, *173* (1-3), 1−38.

(28) Kim, J. M.; Chang, S. M.; Kong, S. M.; Kim, K. S.; Kim, J.; Kim, W. S. Control of Hydroxyl Group Content in Silica Particle Synthesized by the Sol-Precipitation Process. *Ceram. Int.* **2009**, *35* (3), 1015−1019.

(29) Bogush, G. H.; Tracy, M. A.; Zukoski, C. F. Preparation of Monodisperse Silica Particles Control of Size and Mass Fraction. *J. Non-Cryst. Solids.* **1988**, *104*, 95−106.

(30) Giesche, H. Synthesis of Monodispersed Silica Powders I. Particle Properties and Reaction Kinetics. *J. Eur. Ceram. Soc.* **1994**, *14*, 189−204.

(31) Wang, H.-C.; Wu, C.-Y.; Chung, C.-C.; Lai, M.-H.; Chung, T.-W. Analysis of Parameters and Interaction between Parameters in Preparation of Uniform Silicon Dioxide Nanoparticles using Response Surface Methodology. *Ind. Eng. Chem. Res.* **2006**, *45* (24), 8043−8048.

(32) Carcouet, C.; van de Put, M. W. P.; Mezari, B.; Magusin, P.; Laven, J.; Bomans, P. H. H.; Friedrich, H.; Esteves, A. C. C.; Sommerdijk, N.; van Benthem, R.; de With, G. Nucleation and Growth of Monodisperse Silica Nanoparticles. *Nano Lett.* **2014**, *14* (3), 1433−1438.

(33) Bogush, G. H.; Zukoski, C. F. Uniform Silica Particle Precipitation: An Aggregative Growth Model. *J. Colloid Interface Sci.* **1991**, *142* (1), 19−34.

(34) Vanblaaderen, A.; Vangeest, J.; Vrij, A. Monodisperse Colloidal Silica Spheres from Tetraalkoxysilanes: Particle Formation and Growth Mechanism. *J. Colloid Interface Sci.* **1992**, *154* (2), 481−501.

(35) Lee, K. T.; Sathyagal, A. N.; McCormick, A. V. A Closer Look at an Aggregation Model of the Stöber Process. *Colloids Surf., A* **1998**, *144* (1-3), 115−125.

(36) Huang, Y.; Pemberton, J. E. Synthesis of Uniform, Spherical Sub-100nm Silica Particles using a Conceptual Modification of the Classic LaMer Model. *Colloids Surf., A* **2010**, *360* (1-3), 175−183.

(37) Green, D. L.; Lin, J. S.; Lam, Y. F.; Hu, M. Z. C.; Schaefer, D. W.; Harris, M. T. Size, Volume Fraction, and Nucleation of Stöber Silica Nanoparticles. *J. Colloid Interface Sci.* **2003**, *266* (2), 346−358.

(38) Matsoukas, T.; Gulari, E. Monomer-Addition Growth with a Slow Initiation Step: A Growth Model for Silica Particles from Alkoxides. *J. Colloid Interface Sci.* **1989**, *132* (1), 13−21.

(39) Sing, K. S. W.; Everett, D. H.; Haul, R. A. W.; Moscou, L.; Pierotti, R. A.; Rouquerol, J.; Siemieniewska, T. Reporting Physisorption Data for Gas Solid Systems with Special Reference to the Determination of Surface Area and Porosity. *Pure Appl. Chem.* **1985**, *57* (4), 603−619.

(40) Landers, J.; Gor, G. Y.; Neimark, A. V. Density Functional Theory Methods for Characterization of Porous Materials. *Colloids Surf., A* **2013**, *437*, 3−32.

(41) Silvestre-Albero, J.; Silvestre-Albero, A.; Rodriguez-Reinoso, F.; Thommes, M. Physical Characterization of Activated Carbons with Narrow Microporosity by Nitrogen (77.4 K), Carbon Dioxide (273 K) and Argon (87.3 K) Adsorption in Combination with Immersion Calorimetry. *Carbon* **2012**, *50* (9), 3128−3133.

(42) Reichenbach, C.; Enke, D.; Moellmer, J.; Klank, D.; Klauck, M.; Kalies, G. Slow Gas Uptake and Low Pressure Hysteresis on Nanoporous Glasses: The Influence of Equilibration Time and Particle Size. *Microporous Mesoporous Mater.* **2013**, *181*, 68−73.

(43) LaMer, V.; Dinegar, R. Theory, Production and Mechanism of Formation of Monodispersed Hydrosols. *J. Am. Chem. Soc.* **1950**, *72* (11), 4847−4854.

(44) Tan, C. G.; Bowen, B. D.; Epstein, N. Production of Monodisperse Colloidal Silica Spheres: Effect of Temperature. *J. Colloid Interface Sci.* **1987**, *118* (1), 290−293.

(45) Pontoni, D.; Narayanan, T.; Rennie, A. R. Time-Resolved SAXS Study of Nucleation and Growth of Silica Colloids. *Langmuir* **2002**, *18* (1), 56−59.

(46) Jafarzadeh, M.; Rahman, I. A.; Sipaut, C. S. Synthesis of Silica Nanoparticles by Modified Sol-Gel Process: The Effect of Mixing Modes of the Reactants and Drying Techniques. *J. Sol-Gel Sci. Technol.* **2009**, *50* (3), 328−336.

(47) Vanblaaderen, A.; Kentgens, A. P. M. Particle Morphology and Chemical Microstructure of Colloidal Silica Spheres made from Alkoxysilanes. *J. Non-Cryst. Solids* **1992**, *149* (3), 161−178.